

A MAP OF DCO^+ 3-2 AND DEUTERATION RATIO IN NGC 1333

By

BRANDON ADAM RAPHAEL

A Thesis Submitted to The Honors College

In Partial Fulfillment of the Bachelors Degree
With Honors in

Astronomy

THE UNIVERSITY OF ARIZONA

AUGUST 2015

Approved by:

Dr. Yancy Shirley
Department of Astronomy

Senior Honors Thesis: A Map of DCO⁺ 3-2 and Deuteration Ratio in NGC 1333

Brandon A. Raphael, Advisor: Yancy L. Shirley

1. Abstract

Deuterium fractionation may prove to be a valuable tracer of the gas associated with the earliest phases of star formation. Specifically, HCO⁺ is an abundant molecule in cold, dense gas clouds in the ISM. The HCO⁺ molecule is deuterated and becomes DCO⁺. NGC 1333, which lies in the Perseus Molecular Cloud, is a well-documented, active protostellar-forming region which may serve as a good platform to test the usefulness of DCO⁺ as a gas tracer. H¹³CO⁺ is known to be sensitive at similar conditions as DCO⁺, thus the ratio of DCO⁺ to H¹³CO⁺, R_D , then provides a method of mapping the Deuterium fractionation. We mapped the NGC 1333 region in the spectral line DCO⁺ 3 – 2 and compare to a previous map of H¹³CO⁺ 3 – 2 to derive R_D . We find a maximum $R_D = 0.140$, with typical values of a few times 0.01 that is comparable to other studies. DCO⁺ emission is extended in this region and correlates well with dust continuum emission, but the Deuterium fractionation was not strongly dependent on peak core location. These results indicate that astrochemical surveys that use pointed observations at core peak locations may miss significant structure in the Deuterium fractionation within molecular clouds.

2. Introduction

Deuterium fractionation may act as a measure of evolution in dense molecular gas. Molecular gas with densities $> 10^3 \text{ cm}^{-3}$ in the ISM is typically rich in the molecular ion Oxomethlium (HCO⁺). In denser and cold gas ($T \leq 30 \text{ K}$), the deuterated version of this molecule, DCO⁺ may also be observed. Mapping this common deuterated molecule may prove it to be an invaluable tool in the study of Deuterium fractionation in early stellar development. The process of fractionation in Deuterated Oxomethlium is generally created by the formation of interstellar ions H₃⁺ and H₂D⁺ from cosmic ray ionization of H₂ and HD followed by the reaction: $\text{H}_2\text{D}^+ + \text{CO} \rightarrow \text{DCO}^+ + \text{H}_2$ (Turner, E. & Zuckerman, B., 1978).

For regions which may contain significant amounts of DCO⁺, NGC 1333 is of extreme interest. This particular object is located in the well studied Perseus Molecular Clouds, which is one of the most active cloud-forming regions in the Gould Belt (Fig. 1; Evans, N., et al., 2014, Table 1). The Gould Belt consists of more than thirty star-forming regions in



Fig. 1.— False-color, optical photograph of the region of interest, NGC 1333. Image credit to Jon Christensen.

the local galactic neighborhood (distance < 900 pc). The Perseus Molecular Cloud exhibits the second largest rate of dense cloud formation—by a significant margin in relation to other clusters in the Gould Belt (Fig. 2). In fact, the Perseus Molecular Cloud is currently one of the fastest producers of Class I objects: a young, deeply embedded phase of star formation (see Evans, II N. J., Dunham, M. M., Jørgensen, K. J., et al. 2009, Fig. 5). This suggests that the Perseus region is currently going through a very active star formation period. Within the Perseus Molecular Cloud, the NGC 1333 region is among the most active sites of current star formation. We previously hypothesized that DCO^+ is a good marker for early stellar formation, thus it is reasonable to expect heavy deuteration to occur within the NGC 1333 making it an object worthy of study and observation.

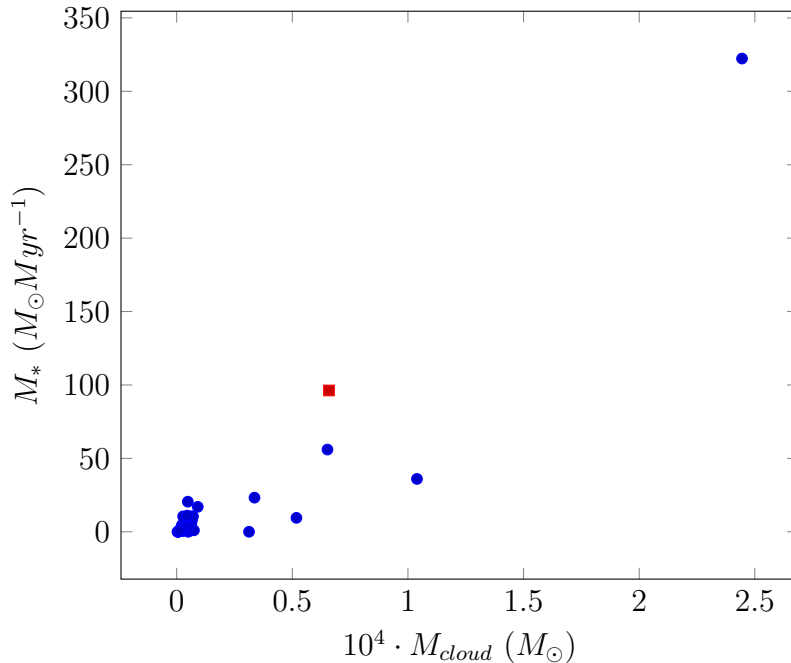


Fig. 2.— Gould Belt Molecular Clouds plotted according to their molecular cloud mass and rate of molecular cloud formation. The red square represents the Perseus Molecular Cloud. While Perseus is not the most massive region, it has the second highest star formation rate of clouds that were studied. Notice the data exhibits a positive correlation. (Evans, N., et al., 2014, Table 1).

In this study, we map the $\text{DCO}^+ 3-2$ emission toward the NGC 1333 region in Perseus. We analyze the Deuterium fraction by comparing to previous observed $\text{H}^{13}\text{CO}^+ 3-2$ to derive the Deuterium fraction ratio, R_D . We compare the extended $\text{DCO}^+ 3-2$ emission with previously published dust continuum observations at 1.1 mm. The dust continuum observations provide a measure of the total amount of material along each line of sight in the NGC 1333 region.

3. Observations

Data collection occurred on Mt. Graham at the Arizona Radio Observatory Heinrich Hertz Submillimeter Telescope (SMT) over 3 nights in February 2014. Using a technique known as On-the-Fly Mapping (OTF), in combination with dual polarization and sideband separation techniques, NGC 1333 was mapped in the $\text{DCO}^+ 3-2$ line at 216.1 GHz in Equatorial coordinates centered at RA: 3:29:04.194, and DEC: +31:16:48.54. Two over-

lapping regions were observed to make a final map with dimensions of $360'' \times 660''$. OTF mapping scans continuously in Right Ascension or Declination at a rate of $10''/s$ while binning together data into 1s spectra. Rows in the OTF map were spaced by $10''$ to produce a heavily oversampled map. OTF maps were alternated scanning in Right Ascension and then Declination to reduce striping in the map.

The 1mm ALMA prototype receiver was used for these observations. The 1mm receiver has two linear polarization feeds – one for Vertical polarization (V_{pol}) and one for Horizontal polarization (H_{pol}). Each detector is sideband separating meaning that two sky frequencies may be observed simultaneously in each polarization. Upper-sideband observations corresponded to $N_2D^+ 3 - 2$ (231 GHz), while lower-sideband observations corresponded to $DCO^+ 3 - 2$. For the purposes of this paper, only the lower side band frequency (216.1 GHz) observations were considered.

4. Analysis

The spectra were scaled and combined to form a corresponding mapping (Fig. 2) to their locations in NGC 1333. In order to accomplish scaling of the spectra, we needed to determine appropriate scale factors for both horizontal and vertical polarizations of the telescope. We first define main beam brightness temperature as:

$$T_{mb} = \frac{T_A^*}{\eta_{mb}} \quad (1)$$

where T_A^* represents the antenna temperature automatically corrected for atmospheric attenuation, η_{mb} represents the efficiency of the main beam (or the fraction of the total beam solid angle within the main beam solid angle), and T_{mb} represents the brightness temperature of the main beam. Using a bright object of known size and flux density to measure T_A^* , the main beam efficiency can then be defined in the following form:

$$\eta_{mb} = \frac{T_A^*(source)}{J(\nu_S, T_{source}) - J(\nu_S, T_{cmb})} \cdot \left[1 - \exp \left(-\ln \frac{2\theta_{eq}\theta_{pol}}{\theta_{mb}^2} \right) \right]^{-1}. \quad (2)$$

$J(\nu, T_B)$ represents the Planck Function for a given frequency and brightness temperature, T_A^* is the calibration source's (in our case, Jupiter's) single-sideband antenna temperature (or scale factor), T_{source} is the brightness temperature of Jupiter, and T_{cmb} is the brightness temperature of the CMB, which is approximately 2.78 Kelvin. θ_{mb} is the full-width half-maximum of our telescope's main beam, θ_{eq} represents Jupiter's equatorial diameter, while θ_{pol} represents Jupiter's poloidal diameter (see Mangum, J. G. 1993, section 3). Using the average T_A^* across the bandpass from Jupiter observations and Equation 2, we were able to

determine the main beam efficiency for both polarizations and both the upper and lower side bands (Table 1). With these efficiencies, we could determine the scale factors for each observation’s data, and combine them into one large data set. Scale factors were produced using equation 1, with the values for η_{mb} being determined by averaging of the common values for the two valid days of observation. The scale factor ($1/\eta_{mb}$) for the vertical polarization of the lower sideband was 1.613, and the scale factor for the horizontal polarization of the lower sideband was 1.515. We could then scale the previously baselined data by using the `@p:scaleall` command in the CLASS software package with the pre-determined scale factors.

	Day 1	Day 2	Day 3
V_{pol} LSB	0.62 ± 0.03	0.43 ± 0.06	0.62 ± 0.04
H_{pol} LSB	0.66 ± 0.04	0.48 ± 0.06	0.66 ± 0.04
V_{pol} USB	0.61 ± 0.03	0.39 ± 0.06	0.62 ± 0.04
H_{pol} USB	0.65 ± 0.04	0.42 ± 0.07	0.65 ± 0.04

Table 1.— Efficiencies for each of the three days of observation using Jupiter. Day 2 efficiencies were far lower than the other days of observation, and inclusion of this data would have been to the detriment of the accuracy of our measurements.

Approximately one-fourth of the initial data was removed from the final data pool. On the second day of observations, cloud coverage prevented appropriate calibration of the telescope using Jupiter, due to a low beam efficiency. Spectral observations of the lower side band frequency were baselined according to a linear fit, specifically using the `@p:baseall` command, with a *baseline* input value of 1 (1 for linear). Baselining removes any continuum signal from the source as well as improper sky subtraction. A linear fit was used, as the spectra were not expected to contain any inherent noise of higher order. These steps were completed through the use of the CLASS software package for Continuum and Line Analysis. Figure 3 shows the results from baselined, calibrated data at the position with the strongest DCO⁺ 3 – 2 emission in the final map.

Once scaled on the T_{mb} temperature scale and baselined, the spectra could be combined using the `@p:combine` command. Care was taken using this tool to not overwrite previously combined data by increasing the scan number index for each new data set to be combined. The data have now been properly calibrated, but the signal-to-noise in any individual spectrum is low because each spectrum is from only 1 second of integration time during OTF binning. Thus, we must average spectra together using an appropriate spatial weighting Kernel in order to re-grid the data onto a regularly-spaced grid and increase the signal-to-noise. We use a Gaussian Convolution Kernel to create the final averaged, gridded data

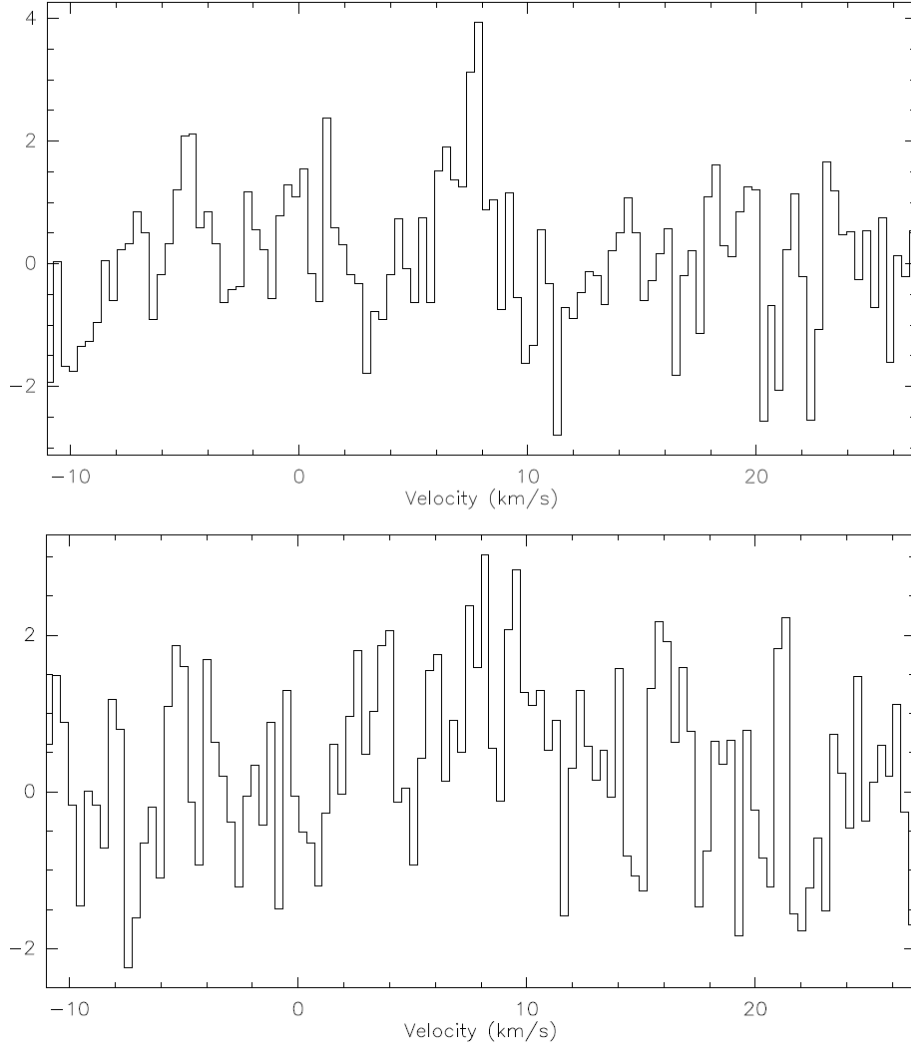


Fig. 3.— Top: Spectral observation of $\text{DCO}^+ 3 - 2$ at 216.1 GHz, corresponding to the horizontal polarization of the lower sideband. Bottom: Spectral observation of $\text{DCO}^+ 3 - 2$ at 216.1 GHz, corresponding to the vertical polarization of the lower sideband. Both images correspond to an offset of $+43.758''$ in Right Ascension and $+85.073''$ in Declination from the center of our observed region. The spectral resolution is 0.35 km/s.

set. The size of the Gaussian Kernel can be obtained by a simple law:

$$(\theta_{res}^{map})^2 = \theta_{fwhm}^2 + \theta_{mb}^2, \quad (3)$$

where θ is the FWHM width of the beams or Kernel. The main beam size (θ_{mb}) was calculated at $34.3''$, and we required a map resolution size (θ_{res}^{map}) of $40''$. This provided a Gaussian Convolution Kernel function with a width of $20.6''$, which was used to average the

scaled spectra. The final map extends 660" in Right-Ascension, and 360" in Declination. Once a Gaussian Kernel width was obtained, we used the `@p:convall` command, with input values of $-180, 180$ (Right Ascension offsets in arcseconds) and $-180, 480$ (Declination offsets in arcseconds). The *Step Size* input was given by the previous Gaussian Kernel width calculation to be 20.6", the *New Beam* input was determined to be 40", and the *BBS* (or old beam size) was determined to be 32.1". We used the *set mode x* and *set mode y* commands with values of 1 and 15, and -1 and 2, respectively. Finally, we used the `@p:mapcso` to create the grid map of spectra of DCO⁺ 3 – 2 emission of NGC 1333, and the *hardcopy* command to create an observable postscript file of this map (Fig. 4).

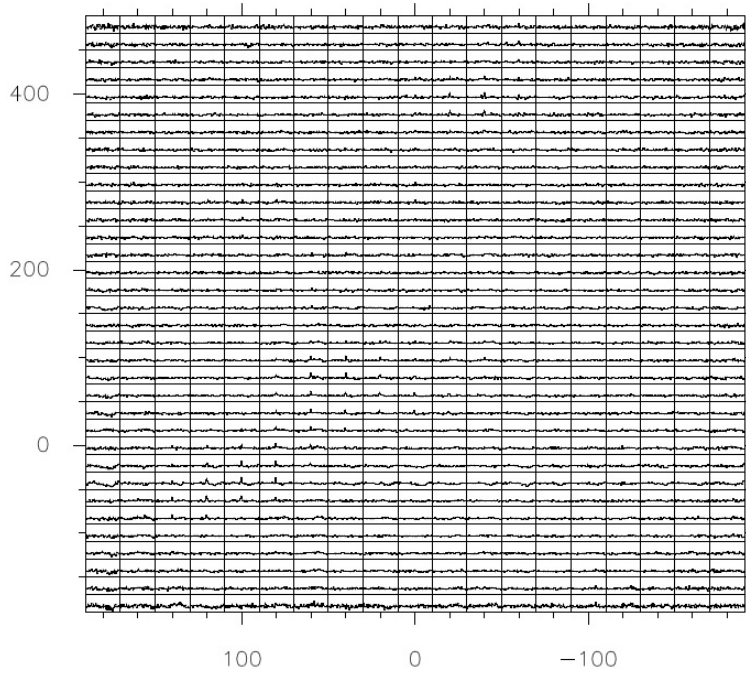


Fig. 4.— Scaled and combined spectra mapped to the NGC 1333 region with 40" resolution. Spectral peaks correspond to detections of DCO⁺, and follow the chevron shape of the region seen in Fig. 4. The map is 660" by 360" in size, centered at RA: 3:29:04.194, and DEC: +31:16:48.54. The baseline r.m.s temperature is 51.0 mK.

Once initial reduction was complete, the ratio of DCO⁺ and H¹³CO⁺ was determined. Integrated intensity of DCO⁺ was taken over a velocity interval from 5 km/s to 11 km/s. Since DCO⁺ emission is expected to be in the optically thin ($\tau_\nu \ll 1$) limit, the column density (see J. G. Mangum & Y. Shirley, 2015, section 11) is given by the following equation:

$$N_{tot}^{thin} = \left(\frac{3h}{8\pi^3 S \mu^2 R_i} \right) \left(\frac{Q_{rot}}{g_J g_K g_L} \right) \left(\frac{\exp\left(\frac{E_u}{kT_{ex}}\right)}{\exp\left(\frac{h\nu}{kT_{ex}}\right) - 1} \right) \left(\frac{1}{(J_\nu(T_{ex}) - J_\nu(T_{bg}))} \int \frac{T_{mb} dv}{f} \right), \quad (4)$$

where h represents Planck’s constant, μ gives the dipole moment, S gives the associated line strength, and R_i gives the relative line strengths. Q_{rot} is the rotational partition function, and $g_J g_K g_L$ are the degeneracies corresponding to energy levels: J , K , and L . E_u represents the upper energy state of our molecular system, k is Boltzmann’s constant, ν is the frequency, and T_{ex} is the excitation temperature defined by Boltzmann’s Equation for the ratio of level populations ($n(J = 3)/n(J = 2) = (7/5) \exp(-h\nu/kT_{ex})$). The $(J_\nu(T_{ex}) - J_\nu(T_{bg}))$ term is derived from the radiative transfer equation, and is assumed to be a constant for our purposes. The integral is used to calculate the integrated intensity, using the T_{mb} as the source main beam radiation temperature, and f as the fraction of the spatial resolution of the measurement filled by the source.

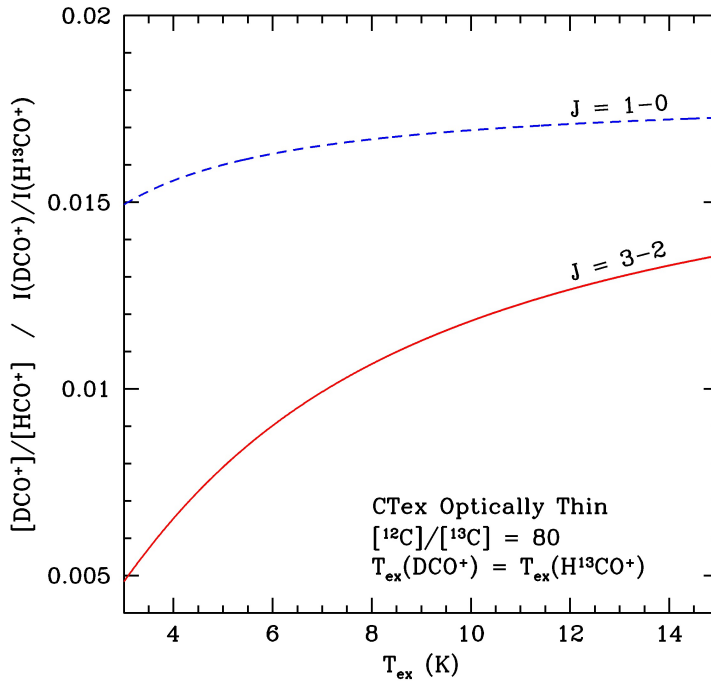


Fig. 5.— Integrated intensity ratio of DCO⁺ to H¹³CO⁺ plotted according to excitation temperature.

In order to determine the regions within NGC 1333 which are very cold and dense, it was necessary to use a similar molecule to compare to DCO⁺. The natural ratio would be to take the ratio of abundance of DCO⁺ to the parent HCO⁺ molecule; however, HCO⁺ emission is typically very optically thick and has no line splitting (i.e. from hyperfine structure) that would make it easy to accurately determine the column density (Shirley et al. 2013). As a result, we use the more optically thin H¹³CO⁺ molecule as a proxy for HCO⁺ with the assumption that the abundance ratio between HCO⁺ and H¹³CO⁺ is 50 : 1. Since

H^{13}CO^+ is less abundant, it is also more likely to have similar excitation conditions to the DCO^+ molecule meaning that we may assume the the excitation temperature for the 3 – 2 transitions of both DCO^+ and H^{13}CO^+ are the same. Figure 5 shows a relation between the ratio of the molecular abundance of DCO^+ and H^{13}CO^+ and their integrated intensities with the excitation temperature that described the level populations of the molecules. We use this relation with an assumption of the excitation temperature (5 K), appropriate for sub-thermally populated gas, to determine the ratio of abundance at each location within NGC 1333. This provides us with a mapping of our region with which we can use to better understand the specific characteristics of Deuteration fractionation (H^{13}CO^+ data from Storm, S., 2014, Private Communication). Assuming an excitation temperature of 5K, a factor of 0.007 is multiplied into the observed integrated intensity ratio to determine the actual abundance ratio of DCO^+ to H^{13}CO^+ , according to the relationship provided in Fig. 5. This ratio is called R_D .

5. Results

Figure 6 shows the final contour map of the DCO^+ 3 – 2 integrated intensity. It is immediately apparent that the DCO^+ emission traces the dust continuum emission well in this region. The 1.1mm dust continuum emission is optically thin at the column densities observed in this region (Shirley et al. 2000); therefore, it traces the total column of material along each line-of-sight. Differences in dust emission intensity are due to either more material along the line-of-sight or hotter material along the line-of-sight. In regions, such as NGC 1333, where embedded protostars are forming and heating the gas, both processes are occurring. The southern half of the dust emission map displays part of a well known chevron shape in the emission with the upper left side of the chevron pattern significantly brighter than the right side. This emission difference is well reflected in the DCO^+ 3 – 2 emission. The brightest DCO^+ emission is also along the upper left side of the chevron feature. Closer inspection reveals that many of the dense cores apparent in the dust continuum map are also apparent in the DCO^+ map. Our first major conclusion is that DCO^+ emission is not just localized to the core peak positions, but is extended in emission over larger portions of the NGC 1333 region. We note that the dust emission map and the DCO^+ 3 – 2 integrated intensity maps have nearly the same angular resolution (33'' versus 40'' respectively).

Figure 7 shows a contour map of the observed R_D ratios in the NGC 1333 cluster. The maximum $R_D = 0.140 \pm 0.021$, and corresponded to the detection of the Perseus-Bolocam 49 protostellar core (Enoch et al. 2008). The average 1σ uncertainty on R_D is 0.025. The contour map of R_D values does not trace the dust emission nearly as well as the DCO^+

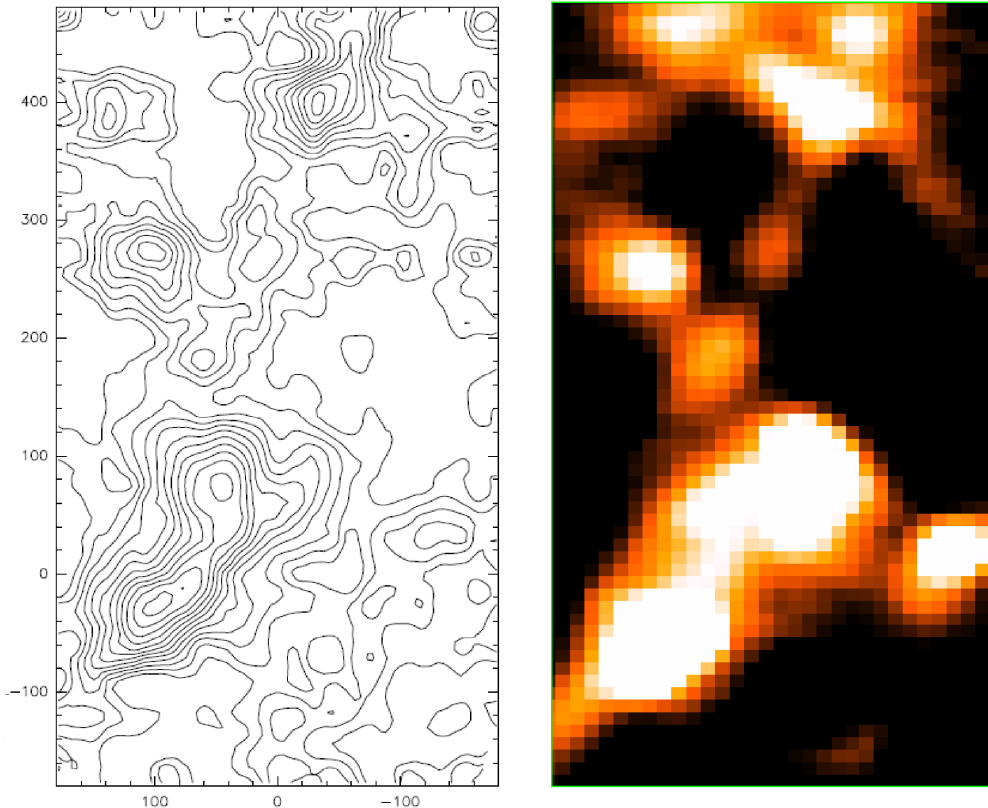


Fig. 6.— Left Panel: Contour map of NGC 1333 of the integrated intensity at 216.1 GHz ($\text{DCO}^+ 3 - 2$). Contour levels are $0.3 (K \cdot km/s)$, which corresponds to three standard deviations of the integrated intensity. Right Panel: An image of the NGC 1333 region taken from the 1.1mm emission Perseus-Bolocam survey (M. Enoch , et al., 2008). Images are of the same scale, and centered at the origin of our survey: RA: 3:29:04.194, DEC: +31:16:48.54.

integrated intensity. This is partially due to lower signal to noise in the $\text{H}^{13}\text{CO}^+ 3 - 2$ map which is used in the ratio to calculate R_D . Obtaining a deeper map in $\text{H}^{13}\text{CO}^+ 3 - 2$ may ameliorate this problem.

The points where R_D is significantly detected are compared to physical quantities derived from previous surveys of the region (see H. Kirk, et al., 2007, Table 1; M. Enoch, et al., 2008, Table 4 and Table 5). These detections were plotted according to their respective R_D values (see Figures 8 and 9). To satisfy as a detection corresponding to a starless or protostellar core, a cutoff of three standard deviations was used. Using that criteria, of the 28 cores within our region, we acquired 12 detections. Of the detections, 10 were protostellar cores, and 2 were starless cores, meaning that those two cores have no indications from

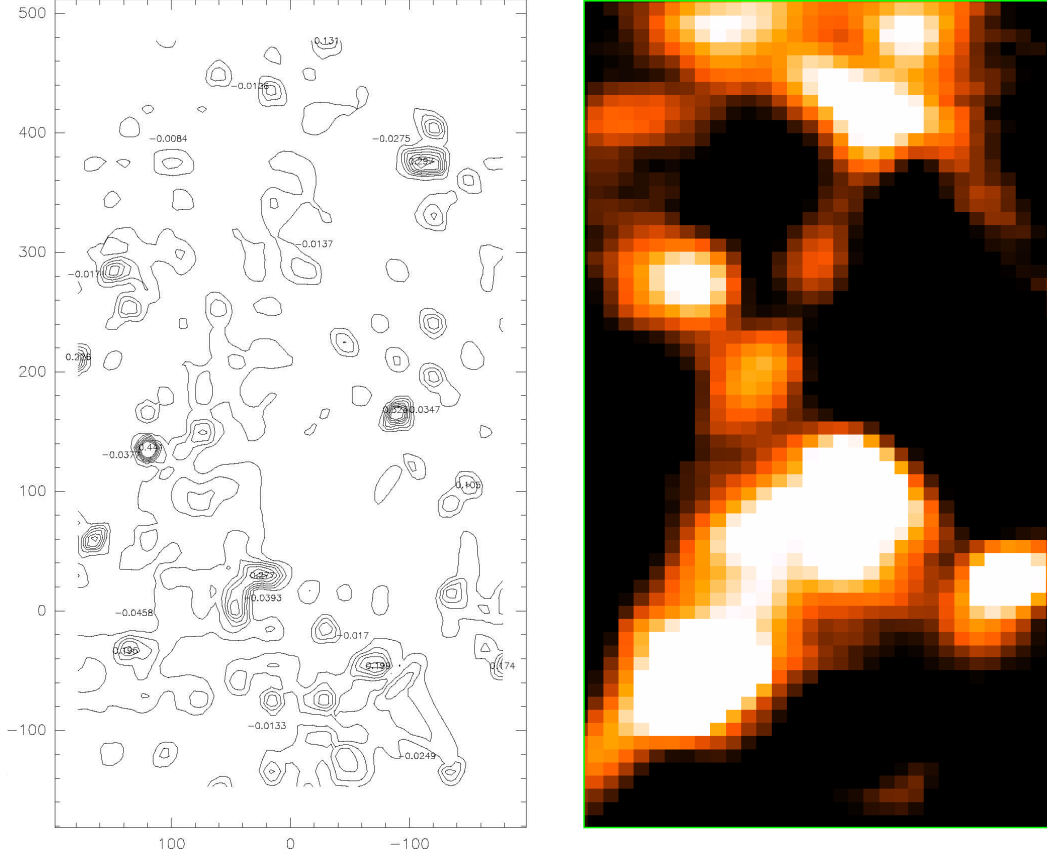


Fig. 7.— Left Panel: A contour mapping of R_D . Contour levels are 0.04 in depth, which corresponds to one standard deviation of R_D . Right Panel: An image of the NGC 1333 region taken from the 1.1mm emission Perseus-Bolocam survey (M. Enoch , et al., 2008). Images are of the same scale, and centered at the origin of our survey: RA: 3:29:04.194, DEC: +31:16:48.54.

infrared surveys of deeply embedded protostellar objects.

Figure 8 shows the plot of core flux values versus the integrated intensity of DCO^+ emission. A weak correlation is observed at these positions. Sources with larger fluxes or flux densities tend to have stronger DCO^+ $3 - 2$ emission. This may in part be due to the excitation conditions required to collisionally excite the $J = 3$ level which is over 25 K above the ground state. Warmer regions will have more collisions and upward collision rates are sensitive to the factor e^{-25/T_k} where T_k is the gas kinetic temperature. Thus, we expect more DCO^+ emission in warmer regions. This process is balanced though by the chemistry. The deuteration reaction that fractionates H_3^+ becomes less efficient above 25 K, driving the DCO^+ abundance down.

Figure 9 shows the plot of the core flux versus the R_D ratio. As with the contour plot of R_D values, no strong correlation is observed. Since the core flux values depend on both the total mass of the clump and the temperature within the clump, this result indicates that Deuterium fractionation observed in DCO^+ is not sensitive to the total mass or temperature in the clumps. Gas kinetic temperature measurements made from NH_3 observations indicate that typical gas temperatures are in the range of 10 – 15 K in the NGC 1333 region (Rosolowsky et al. 2008). Unfortunately, there is not enough dynamic range in T_k to test how the R_D ratio varies with T_k (see Friesen et al. 2013 for an illustration of the problem for all of Perseus).

6. Conclusions

DCO^+ is present as an extended emission source in NGC 1333 that appears well correlated with dust continuum emission on a large scale (Fig. 6). The ratio of DCO^+ to H^{13}CO^+ is not well correlated with the location of the dense cores although the low signal to noise of the comparison H^{13}CO^+ map presents difficulties in the final R_D map (Fig. 7). This is a similar finding to a previous study performed on the Perseus Cluster (Friesen, R. K., Kirk, H. M., & Shirley, Y. L. 2013). Although we see a slight correlation between DCO^+ integrated intensity and the core peak fluxes, there is no correlation observed between R_D and core peak fluxes. Our study indicates that the geometrical distribution of a common deuterated species such as DCO^+ are more complicated. Simple surveys of core peak positions in this molecule will fail to capture the nature of emission and may misinterpret the astrochemistry of these regions. Mapping the emission is necessary and quite easy. The 66 square arcminute map presented here only required 16 hours of observing time.

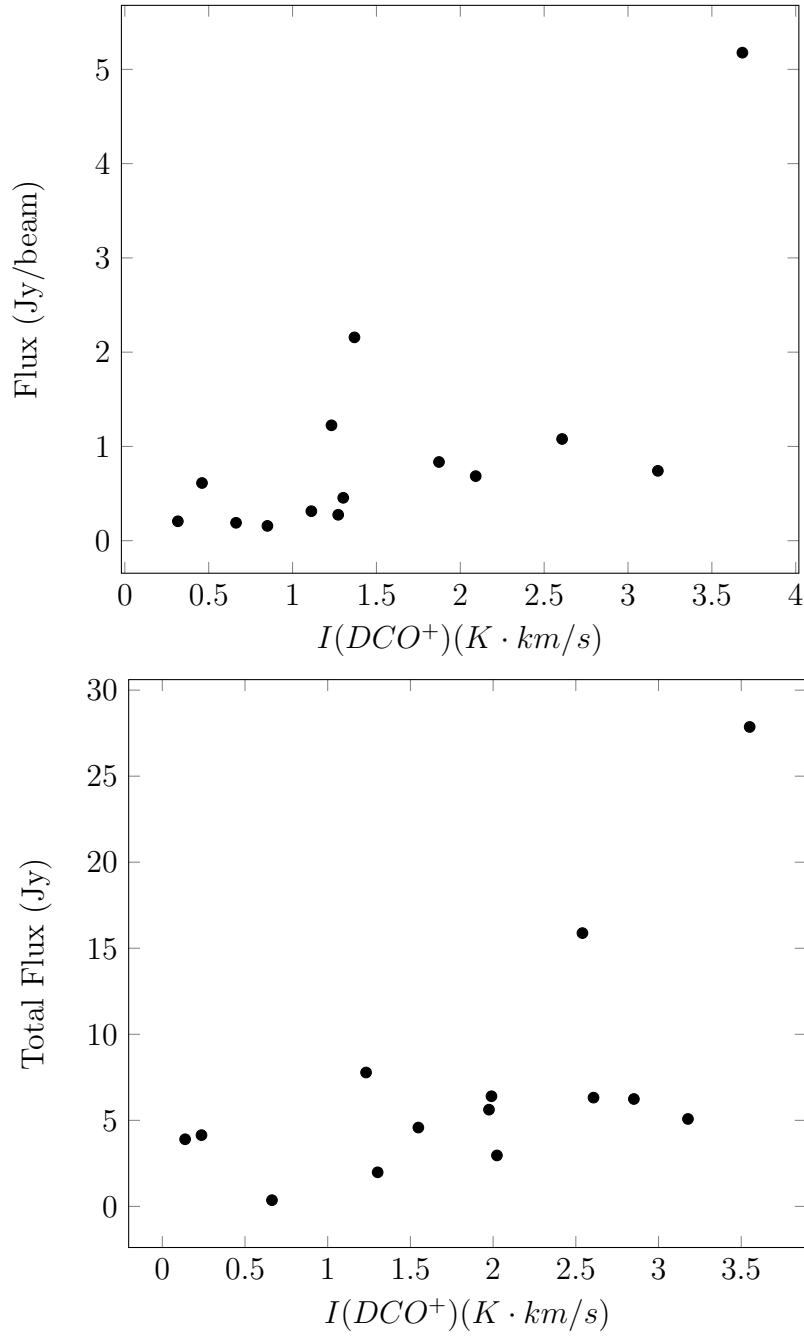


Fig. 8.— Top: The observed flux is plotted according to the observed integrated intensity of DCO^+ for the Perseus-Bolocam cores. Bottom: The total flux is plotted according to the integrated intensity of DCO^+ for the SCUBA cores.

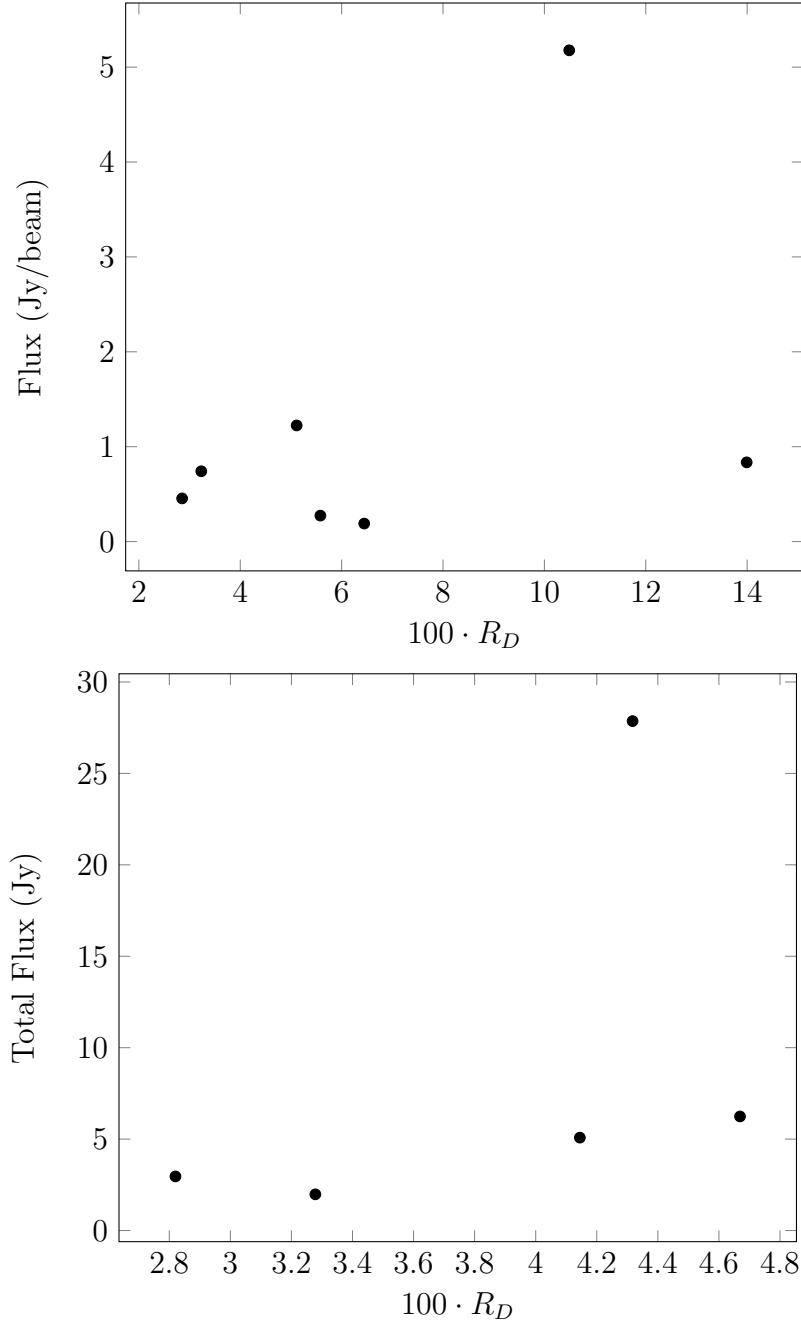


Fig. 9.— Top: The observed flux is plotted according to the observed R_D value for Perseus-Bolocam core observations, both starless and protostellar. Bottom: The total flux is plotted according to the R_D value for SCUBA core observations.

ID	RA	DEC	Flux(Jy/beam)	R_D
Per-Bolo 38	3:28:55.3	+31:14:32	1.224	0.051 ± 0.0337
Per-Bolo 41	3:29:00.6	+31:11:59	0.190	0.064 ± 0.0264
Per-Bolo 44	3:29:04.5	+31:18:42	0.274	0.055 ± 0.0177
Per-Bolo 45	3:29:07.7	+31:17:17	0.455	0.028 ± 0.0196
Per-Bolo 46	3:29:08.3	+31:15:11	0.741	0.032 ± 0.0277
Per-Bolo 48	3:29:10.9	+31:13:26	5.177	0.104 ± 0.0285
Per-Bolo 49	3:29:11.3	+31:18:25	0.835	0.140 ± 0.0211

Table 2.— Deuteration ratios taken from the mapping shown in Figure 4 for Perseus-Bolocam cores.

ID	RA	DEC	Flux(Jy)	R_D
SCUBA 106	3:29:09.9	+31:13:31.1	27.86	0.043 ± 0.0282
SCUBA 107	3:29:08.8	+31:15:12.8	5.08	0.041 ± 0.0308
SCUBA 109	3:29:06.8	+31:17:18.3	1.98	0.032 ± 0.0164
SCUBA 110	3:29:06.5	+31:15:36.3	6.24	0.047 ± 0.0282
SCUBA 111	3:29:03.7	+31:14:47.7	2.96	0.028 ± 0.0249

Table 3.— Deuteration ratios taken from the mapping shown in Figure 4 for SCUBA cores.

REFERENCES

- Enoch, M. L., Evans, II N. J., Sargent, A. I., Glenn, J., Rosolowsky, E., & Myers, P. 2008, *ApJ*, 684, 1240
- Evans, II N. J., Dunham, M. M., Jørgensen, K. J., et al. 2009, *ApJS*, 181, 321
- Evans, II N. J., Heiderman, A., & Vutisalchavakul, N. 2014, *ApJ*, 782, 114
- Friesen, R. K., Kirk, H. M., & Shirley, Y. L. 2013, *ApJ*, 765, 59
- Kirk, H., Johnstone, D., & Tafalla, M. 2007, *Astrophys. J.*, 668, 1042
- Mangum, J. G. 1993, *PASP*, 105, 117
- Mangum, J. G., & Shirley, Y. L. 2015, *PASP*, 127, 266
- Rosolowsky, E. W., Pineda, J. E., Foster, J. B., et al. 2008, *ApJS*, 175, 509
- Shirley, Y. L., Ellsworth-Bowers, T. P., Svoboda, B., et al. 2013, *ApJS*, 209, 2
- Shirley, Y. L., Evans, II N. J., Rawlings, J. M. C., & Gregersen, E. M. 2000, *ApJS*, 131, 249

Storm, S., Private Communication, 2014

Turner, B. E., & Zuckerman, B. 1978, ApJ, 225, L75